COVARIANCE OF NONSTATIONARY SODIUM CURRENT FLUCTUATIONS AT THE NODE OF RANVIER

FREDERICK J. SIGWORTH, *Department of Physiology, Yale University School of Medicine, New Haven, Connecticut 06510 U.S.A.*

ABSTRACT A theory is presented which relates the nonstationary autocovariance (covariance) function to the kinetics of independently-gated ionic channels. The experimental covariance was calculated from ensembles of 256–504 current records elicited from single, voltage-clamped, frog myelinated nerve fibers. Analysis of the covariance shows that the decay of channels from conducting to nonconducting states proceeds more slowly late in a depolarization to near 0 mV, as compared with early in the same depolarization. This behavior is inconsistent with there being only one kinetic state corresponding to the open channel. The behavior can be explained by the existence of multiple kinetic states corresponding to the open channel, or, alternatively, by the existence of multiple, kinetically distinct populations of channels.

INTRODUCTION

A formal procedure for developing a model for voltage-dependent conformational changes in ionic channels has been proposed by Stevens (1978). The first step of that procedure is to identify the kinetic states of the channel and to determine the conductance level associated with each state. In the case of the sodium channel in the node of Ranvier, it is now apparent that there are only two conductance levels, corresponding to "open" or "closed" channels (Sigworth, 1980*a*; Conti et al., 1976*a*,*b*; Hille, 1976). It is not known, however, how many kinetic states correspond to the "open" channel.The usual interpretation of the Hodgkin-Huxley equations, for example, has only one open state which corresponds to having the h and m gates all in their permissive states. Recently, theories of gating have been proposed by Armstrong and Benzanilla (1977) and Neumcke et al. (1978) that postulate multiple open states on the basis of the observed kinetics of gating charge movement. The goal of the present work is to test for the possibility of multiple open states using fluctuation analysis.

The method employed here is an extension of a technique that was reported previously (Sigworth, 1977; 1980*a*,*b*). In the previous work the size of fluctuations within an ensemble of sodium current records was used to determine the single-channel conductance and other properties of sodium channels in the node of Ranvier. This paper considers the temporal structure of the fluctuations, which is described by a two-dimensional autocovariance function (hereafter called covariance). On the basis of certain assumptions this function will be shown to be simply related to the conditional probability that a channel is open at one time, given

---

Dr. Sigworth's present address is Max Planck Institut für Biophysikalische Chemie, Postfach 968, D-3400 Göttingen, Federal Republic of Germany.

that it is open at another time. This analysis will then be applied to the fluctuations, mainly from inactivation, in sodium currents in the limited potential range of -15 to +5 mV. This range is in the region where inactivation shows multi-component behavior (Chiu, 1977). The multi-component behavior is particularly interesting in this study because it can be explained by theories assuming one open state, multiple open states, or multiple populations of channels. The technique presented here can distinguish at least partially among these alternatives.

THEORY

The power spectrum and its dual, the stationary covariance function, have been used extensively to provide information about the kinetics of gating of individual ionic channels (see reviews by Neher and Stevens, 1977; DeFelice, 1977; Conti and Wanke, 1975). Stevens (1972) and Hill and Chen (1972) have shown that these descriptions of the temporal structure of current noise have a simple interpretation when channels are assumed to have only two levels of conductance (open and closed). In this case the time-course of the covariance is proportional, except for a constant term, to the average time-course of the "decay" of a channel from being open to its final equilibrium among open and closed states. However, since it is a time average, the stationary covariance has a simple meaning only if the membrane current is constant with time.

The temporal structure of fluctuations from a nonstationary process is better described by the two-dimensional covariance function (Bendat and Piersol, 1971; Papoulis, 1965) which quantifies the correlation between fluctuations at two different times. Like the stationary covariance, the nonstationary form can provide information about the kinetics of individual channels. Because it is not a time-average, however, it contains additional information about possible changes in the channel kinetics with time during the gating process.

The Covariance for Identical, Independent Channels

To derive theoretical expression for the covariance, it is first assumed that the channels in the patch of membrane under study are gated independently and that they form a homogeneous population. These assumptions allow us to calculate the covariance for a single channel and then multiply it by the number of channels to obtain the covariance of the membrane current. The independence of gating is supported by previous work (Sigworth, 1980*b*). The assumption of homogeneity (that all channels have the same gating kinetics) might not hold for nerve membranes, but if it does not, the covariance for each population of channels can in principle be estimated, and the results summed.

Let $y(t)$ be the fluctuating current through one channel. Its ensemble expectation value is

$$\mu(t) = \langle y(t) \rangle = \sum_{ij} p_j(t) i_j, \tag{1}$$

a sum over the various possible single-channel current levels i_j weighted by the probabilities p_j of being in these states. The covariance of y for N channels is given by

$$\begin{aligned} c(t_1, t_2) &= N\langle [y(t_1) - \mu(t_1)][y(t_2) - \mu(t_2)] \rangle \\ &= N \sum_k \sum_j p_j(t_1) p_{kj}(t_2 \mid t_1)[i_j - \mu(t_1)][i_k - \mu(t_2)], \end{aligned} \tag{2}$$

where $p_{kj}(t_2 | t_1)$ is the conditional probability of being in state k at time t_2, given that the channel is in state j at t_1. Expanding the product of terms at the right and using the identity

$$\sum p_j(t_1)p_{kj}(t_2 | t_1) = p_k(t_2),$$

we have

$$C(t_1, t_2) = N \sum_k \sum_j p_j(t_1)p_{jk}(t_2 | t_1) [i_j i_k - i_j \mu(t_2)]. \tag{3}$$

This is the covariance for one channel having any number of conductance levels.

Two Conductance Levels

Conti et al. (1980) have presented the expression for C with currents $i_0 = 0$ and $i_1 = i$. In this case $\mu(t) = ip(t)$, where $p = p_1$ is the probability of being in the open state 1. By using the identity $p_{01}(t_2 | t_1) = 1 - p_{11}(t_2 | t_1)$, Eq. 3 simplifies to

$$\begin{aligned} C(t_1, t_2) &= Ni^2 \sum_{k=0}^{1} p(t_1)p_{k1}(t_2 | t_1)[i_k - ip(t_2)] \\ &= Ni^2 p(t_1)[p_{11}(t_2 | t_1) - p(t_2)], \end{aligned} \tag{4}$$

which is symmetrical under the interchange of the time variables t_1 and t_2.

As a check, the covariance function can be evaluated at $t_1 = t_2$

$$C(t_1, t_1) = Ni^2 p(t_1) [1 - p(t_1)] = \sigma^2(t_1), \tag{5}$$

and is seen to yield the variance (Ehrenstein et al., 1970).

The Significance of p_{11}: One Open State

We now make the usual assumption (Colquhoun and Hawkes, 1977; Stevens, 1978) that channel gating is a Markov process with potential-dependent, time-homogeneous transition probabilities. The time independence of the transition probabilities allows us to call them "rate constants." The Markov assumption means that at a constant potential the behavior of an individual channel in the future depends only on which state it is in at the present, and the values of the rate constants. Further, it means that at at given potential the behavior of a channel , once it is in a given state s, does not depend on the time of arrival in s or the pathway by which it reached s. Hodgkin-Huxley kinetics is a process of this kind where, for example, one specific state would correspond to two m "gates" open, one m "gate" closed, and the h "gate" open.

In this framework p_{11} has a simple meaning in the case of one open state of the channel . Let s be the open state. Then for $t_2 > t_1$, $p_{11}(t_2 | t_1)$ is the probability that the channel is in s at t_2 given that it was in s at t_1. By the Markov assumption this conditional probability depends only on the delay between t_1 and t_2 at constant potential.

$$p_{11}(t_2 | t_1) = p_{11}(t_2 - t_1 | 0), t_2 \geq t_1 . \tag{6}$$

This function is the normalized time-course of the conductance decay we would measure if we could place each channel in the membrane into state s and then allow the channels to relax at a fixed potential.

The behavior of p_{11} for times $t_2 < t_1$ can be calculated using Bayes' rule

$$p_{11}(t_2 | t_1) = [p(t_2)/p(t_1)]\, p_{11}(t_1 | t_2)\,, \tag{7}$$

where p is the simple probability of being in the open state, as before. If the process is stationary, then p is a constant, and $p_{11}\ (t_1+\tau | t_1)$ is independent of t_1 and has the symmetry property $p_{11}(t_1+\tau | t_1) = p_{11}\ (t_1-\tau | t_1)$. This symmetry is also present in the stationary covariance function (Stevens, 1972; Hill and Chen, 1972)

$$C(\tau) = Ni^2 p\, [p_{11}(\tau | 0) - p]\,, \tag{8}$$

which is a special case of Eq. 4.

Multiple Open States

If there is more than one open state of the channel, then p_{11} has a more complicated form. In the general case where the various open states have different conductances, Eq. 3 must be used to calculate the covariance, using the probability functions for each state. If all of the open states have the same conductance, then Eq. 4 can also be used if p_{11} is defined to be the probability that a channel is in any open state at t_2, given that it is in any open state at t_1:

$$p_{11}(t_2 | t_1) = \frac{\sum_k \sum_j p_j(t_1) p_{kj}(t_2 | t_1)}{\sum_k p_k(t_2)}\,. \tag{9}$$

Here all of the sums are taken only over the open states; the denominator is therefore the probability of a channel being open at t_2, and each term in the numerator is a joint probability of a channel being open both at t_1 and t_2. Once again the Markov assumption means that the individual conditional probabilities $p_{kj}(t_2 | t_1)$ depend only on the time difference for $t_2 \geqslant t_1$, and Bayes' rule (Eq. 7) gives $p_{11}(t_2 | t_1)$ for $t_2 < t_1$ as before. When the p_j are constant, the process is stationary and p_{11} is symmetrical about t; the stationary covariance is again given by Eq. 9.

If the p_j are time-varying, $p_{11}(t_1+\tau | t_1)$ will not only be asymmetric in τ, but will also in general show a variable decay time-course for $\tau \geqslant 0$ that depends on t_1, as well as τ. This latter variation arises because the p_j are the weights of the various decay modes in the sum in Eq. 9. Since no variation with t_1 can occur in the case of one open state, the experimental evaluation of p_{11} under different initial conditions and at different t_1 values can provide a test for multiple open states with different decay kinetics.

Strategy for the Experiments

One strategy to test for multiple open states of a channel population is clear from the results of the previous section. The steps are: (*a*) Collect an ensemble of current records elicited by identical pulse patterns and calculate the covariance C from the fluctuations. (*b*) Use Eq. 4 to calculate the conditional probability p_{11} from the experimental C values. (*c*) Observe the decay of p_{11}. If the decay shows significant variations in time-course at the same potential, the hypothesis of one open state of the channel is shown to be false.

The experimental program described below follows this strategy. Technically, the best fluctuation data could be obtained in the restricted potential range of -15 to +5 mV and at

low time resolution (a sampling interval of 200 μs was used in most cases). Because activation is both rapid and nearly complete in this potential range, only small and poorly resolved fluctuation components are expected from that process. Therefore this study is concerned primarily with the inactivation process.

Inactivation in the node of Ranvier is itself interesting in two respects. First, Armstrong and Bezanilla (1977) have postulated a second open state of the sodium channel in squid axons to explain a slow gating-current component that appears to flow after the channels have opened. In their model, the transition into this state is the first step toward inactivation at depolarized potentials like those used here. A second open state of this sort should be detectable by the method that has been outlined. Second, inactivation in the node of Ranvier does not follow a single-exponential time-course, but can be better described by a sum of two or more exponential components (Chiu, 1977; Nonner, 1980). Chiu has described this behavior by a two-step inactivation process, while Nonner's theory includes three steps and describes the immobilization of the gating charge as well. Both of these theories postulate only one open state, although other schemes could be imagined that include multiple open states or multiple populations of channels to account for the various components in the inactivation time-course. Thus an independent test for multiple open states in the node of Ranvier sodium channels would help narrow the range of possible theories of channel gating.

EXPERIMENTAL METHODS

Preparation and Voltage Clamp

Some of the experiments described here were performed concurrently with those in a previous paper (Sigworth, 1980*a*), and the basic properties of these nerve fiber preparations, which were from *Rana pipiens*, are given in Table 1 of that paper. Other fibers (Nos. 54–58) were from *Rana catesbiana*. They

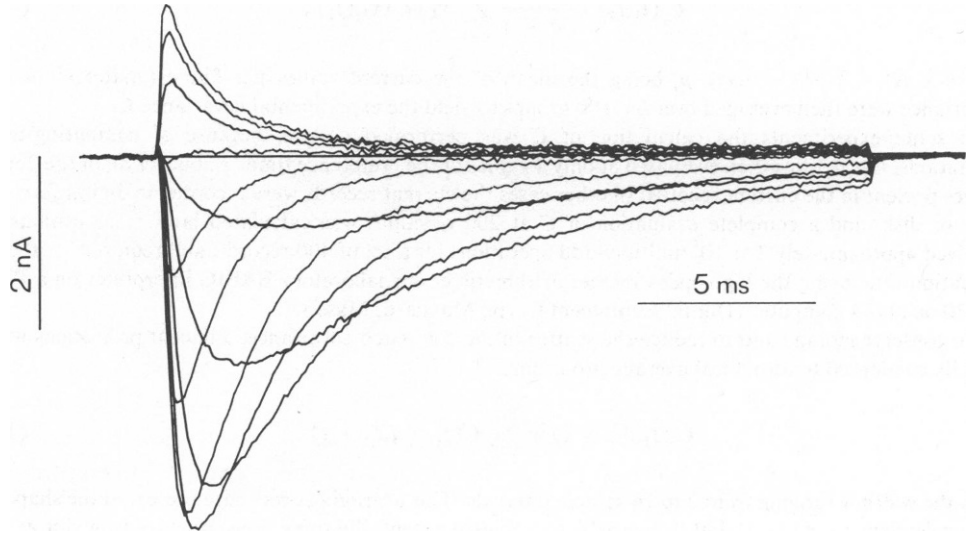

FIGURE 1 Na^+ currents in fiber 56. 20-ms depolarizations were given after 50-ms hyperpolarizing pulses to -105 mV. The current signal was filtered at 5 KHz (Bessel response) and sampled at 100 μs intervals. The test potentials were -35, -25, -15, -5, 5, 25, 45, 65, 85, 105, and 125 mV. The reversal potential was very near 65 mV. No series-resistance compensation was used.

averaged 16 μm in diameter, had sodium reversal potentials averaging 60 mV, and had an average single Na-channel conductance of 7.0 ± 0.3 pS near 4°C, which is essentially identical to the value obtained in *R. temporaria* and *R. pipiens* under the same conditions. These fibers showed relatively smooth reversal of the currents (Fig. 1) and a clear slow component of inactivation at potentials in the range of -25 to +25 mV (Figs. 1 and 6).

The voltage clamp and other equipment have been described previously (Sigworth, 1980*a*). Single nodes of Ranvier in these nerve fibres were voltage clamped at 3–5°C; the ends of the fibres were in pools containing (concentrations in mM) 20 NaCl and 100 CsCl. The solution bathing the node was 100 NaCl, 20 tetraethylammonium-Cl, 5 Hepes, and 1.8 CaCl at pH = 7.4. A series resistance compensation value of $0.01 \times R_{ED} \simeq 0.3$ MΩ was used except where noted. The membrane current signal was usually filtered at 2 or 5 kHz (−3 dB frequency; 4 pole, Bessel response) and sampled at intervals of 0.2 or 0.1 ms. Scaled records from hyperpolarizations (typically to -115 mV) were used to correct for leakage and capacitance currents. The covariance and other statistical quantities were computed digitally from sets of 256–504 current records, each 256 samples long, elicited by identical pulse patterns applied at intervals of 400–600 ms. As in the previous work, care was taken to make the relative timing of the stimulus and the sampling of the current records repeatable to <20 ns. The holding potential was -75 mV.

Computation of C and p_{11}

The nonstationary covariance functions would ideally be estimated as the expectation value over a large ensemble of current records

$$C(t_1,t_2) = \langle x(t_1)x(t_2) \rangle , \tag{10}$$

where $x(t) = y(t) - \mu(t)$ is the deviation of the current $y(t)$ from its ensemble mean value. In practice, the mean current time-course $\mu(t)$, deviations $x(t)$, and covariance $C(t_1,t_2)$ were calculated in groups of n = 4 or 6 records to avoid the effects of long-term changes in the currents (see below). For the jth group, the covariance was estimated as

$$C_j(t_1,t_2) = \frac{1}{n-1} \sum_{k=1}^{n} x_{kj}(t_1)x_{kj}(t_2) , \tag{11}$$

where $x_{kj}(t) = y_{kj}(t) - \mu_j(t)$, μ_j being the mean of the current values y_{kj}. The estimates C_j of the covariance were then averaged over 64–100 groups to yield the experimental covariance C.

In some experiments the calculation of C was performed on-line; because of computing-time limitations, $C(t_1,t_2)$ was then evaluated at only 4 values of the "reference time" t_1, but for all of the 256 t_2 values present in the current records. In other cases the current records were recorded in digital form on tape or disk, and a complete evaluation of C at 200 t_1 values was calculated later. This evaluation involved approximately 2×10^7 multiply-add operations for a set of 400 records, and required ~ 30 min execution time using the high-speed integer arithmetic of our laboratory BASIC interpreter on a PDP 11/20 or 11/34 computer (Digital Equipment Corp., Maynard, Mass.).

To conserve storage and to reduce the scatter in the computed covariance, adjacent projections were usually condensed to form local average projections

$$C(t_1,t_2) = 1/w \sum_{i=0}^{w-1} C(t_1 + i, t_2 + i) , \tag{12}$$

with the width w ranging from 2 to 16 sample intervals. This averaging procedure preserved the shape of the projections near $t_1 = t_2$, but "smeared," to a limited extent, the rapid nonstationary behavior at the beginning of the depolarizations. The computation of theoretical curves included the same averaging procedure to allow direct comparison with the experimental data.

p_{11} was calculated from the experimental values of the covariance C by using Eq. 4 and the expression

$p(t) = I(t)/Ni$, where I is the mean membrane current:

$$p_{11}(t_2|t_1) = \frac{C(t_1, t_2)}{Ni^2 p(t_1)} + p(t_2) = \frac{C(t_1, t_2)}{iI(t_1)} + \frac{I(t_2)}{Ni}. \quad (13)$$

Thus p_{11} was calculated as the covariance, normalized by a factor proportional to mean current at t_1 with an added correction term equal to the probability of channels being open at t_2. This term is largest when t_2 is the time of the peak current, and in most of these experiments it had a maximum value $p_{max} \simeq 0.5$. The parameters N and i were chosen by the criterion that $p_{11}(t_1|t_1) = 1$ for all values of t_1. This is equivalent to fitting the variance-mean relationship (Eq. 5) and always gave values close to those obtained by that procedure (Sigworth, 1980 *a,b*).

Effect of Drift

The group-wise computation of the covariance was designed to minimize the effect of long-term changes in the sodium current (Sigworth, 1980*a*). The residual effect of a relative amplitude change δ between records is to add an error component C_{drift} the computed covariance,

$$C_{drift}(t_1,t_2) = k_n \delta^2 I(t_1) I(t_2), \quad (14)$$

where k_n is a constant depending on the group size n, and is ~1.7 and 3.5 for $n = 4$ and 6, respectively. Adding this component to C in Eq. 13 has the same effect as altering N to an apparent value $N' = N/(1+k_n N\delta^2)$. Since the value of N' is determined by fitting the same set of fluctuation data, no error results in the estimation of p_{11} in the case of simple run-down. Since $\delta \ll 10^{-4}$ in these experiments, the relative error $k_n N \delta^2$ was always $< 10^{-3}$, much smaller than the uncertainty of ~5% in determinations of N.

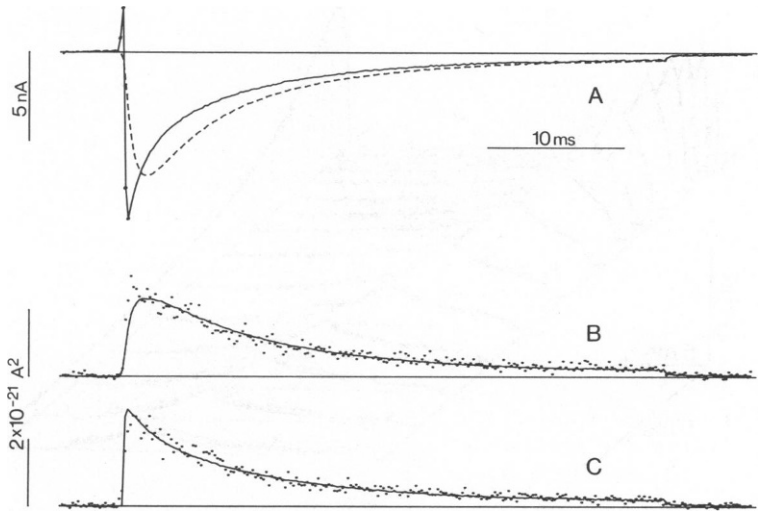

FIGURE 2 Mean current and variance records for tails and steady depolarizations in fiber 58. 50-ms prepulses to -105-mV were given in each case. (*A*) Mean currents. Solid curve is the tail current elicited by a 0.2-ms activating pulse to +125 mV followed by 19.8 ms at -5 mV. Currents during the activating pulse are poorly resolved (discrete samples are indicated by dots). Dashed curve is from a corresponding step depolarization to -5 mV. (*B*) Variance during step depolarizations, after subtraction of the estimated background variance (Sigworth, 1980*a*). Smooth curve is the predicted variance derived from the mean with i = -0.49 pA, N = 49,000. (*C*) Variance during tail currents. Smooth curve is drawn with the same parameters as in *B*. Currents were filtered at 5 kHz and sampled at 100-μs intervals.

RESULTS

The covariance was evaluated in currents from step depolarizations and from "tail currents" elicited by short, large depolarizations (200–400 μs at +125 mV) returning to less depolarized test potentials. Fig. 2 shows the currents and the time-course of the variance elicited by these two pulse patterns with a test potential of -5 mV in each case. As can be seen in parts *B* and *C* of the figure, the variance-mean relationship from the two pulse patterns can be fitted with the same values of N and i.

In the experiments described in this paper, test potentials were chosen in the range -15 to +5 mV, which was constrained by several factors. First, the inactivation time-course in this range is well described by a sum of two or more exponentials; at larger depolarizations the slower component has a smaller amplitude (Chiu,1977). Second, the single-channel current is large enough (on the order of -0.4 pA) to provide usable fluctuations. Third, the voltage-dependence of activation is not steep in this region. This lessens the possibility of excess fluctuations from the regenerative effects of series resistance or from gating fluctuations driven by noise in the clamped membrane potential (Sigworth, 1979; 1980*a*).

Fig. 3 illustrates the covariance calculated from 390 step depolarizations to -5 mV. The time-course of the mean conductance is shown to the right, and the vertical dotted lines indicate the reference times t_1 for each projection of the covariance. For a stationary process, each projection of the covariance is expected to be symmetrical in t_2 about the point $t_2 = t_1$. The early projections demonstrate clearly nonstationary behavior, with very different rising

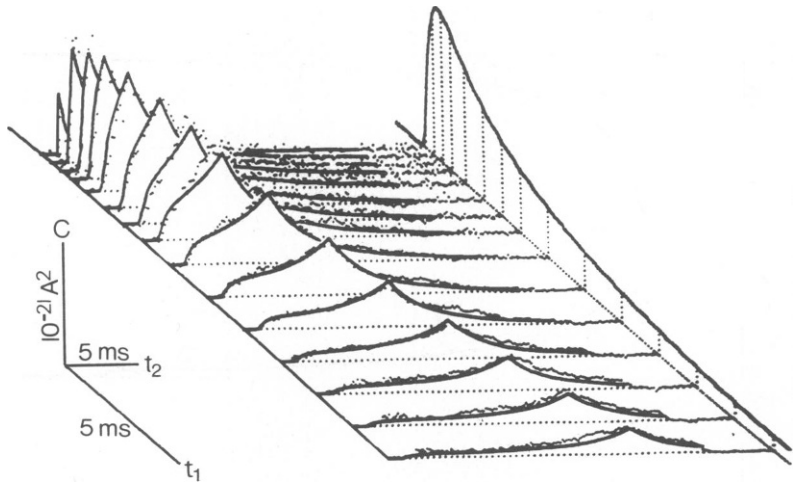

FIGURE 3 Three-dimensional plot of $C(t_1,t_2)$ calculated from 65 groups of 6 depolarizations to -5 mV in fiber 30. 50-ms, -105-mV prepulses were used. The magnitude of C is the vertical dimension, and the two time variables t_1 and t_2 are the horizontal dimensions. Note that t_1 has a much larger scale factor. The corresponding mean-current time-course is plotted to the right as a function of t_1. The vertical dotted lines indicate the starting times t_1 at which each of the averaged projections $C_w(t_1,t_2)$ was evaluated. The values of the averaging width w were 2 for the first four projections, 4 for the next four projections, and 8 for the last seven projections. Only half of the computed projections are shown for clarity. The solid curves are the predictions of the one-open-state scheme A with i = -0.34 pA, N = 50,000, λ_1^{-1} = 0.27 ms, λ_2^{-1} = 1.9 ms, λ_1^{-1} = 6.1 ms, b_α' = 0.04, b_2' = 0.56, b_3' = 0.4, and the activation parameter $\alpha_m/(\alpha_m + \beta_m)$ = 0.95.

and falling phases, while the later projections become more symmetrical as the mean conductance approaches a small steady value.

For clarity the data points at $t_2 = t_1$ are not plotted in the figure; Fig. 1 of Sigworth (1980*b*) shows similar data with these points plotted. They represent a narrow spike resulting from the thermal noise background and are 3–7 $\times$ 10^{-22} A^2 above the extrapolated peaks shown in the figure. The background noise has a spectral density of the form $S_I = S_o(G_m) + S_1 f^2$ that depends on the instantaneous membrane conductance G_m (Sigworth, 1979;1980*a*); when this noise is processed by the low-pass filter it results in a covariance component

$$C_{th}(t_1,t_1+\tau) = S_o(G_m)\, R(\tau) + S_1 R''(\tau), \qquad (15)$$

where R is the autocorrelation of the filter's impulse response, and R'' is the second derivative. At the 2-kHz filter setting R had a width at half-maximum of 105 μs which, because it was much less than the 200 μs sampling interval, caused only the points at $t_2 = t_1$ to be affected.

Three characteristics of the experimental covariance suggest that it arises primarily from the gating of sodium channels. First, there was essentially no correlation between fluctuations at rest and during the depolarizations (Fig. 4 *A*). The covariance vanished whenever one of the time variables was chosen before or after the depolarization, and the fluctuations at the holding potential showed only the thermal-noise spike. The lack of correlations argues against the presence of excess fluctuations from leakage channels, and is a strong test for the stability of the clamped membrane potential.

Second, at the sodium current reversal potential (Fig. 4 *B* the only feature in the covariance was a spike at $t_2 = t_1$. The lack of any slowly varying component shows that the contribution from fluctuations in other ionic conductances is negligible. Third, the form of the covariance did not change when the sodium current was reduced using small doses of toxins or depolarizing prepulses. Reducing the current reduces the relative contributions from many sources of artifacts, including timing jitter, series resistance, and the voltage driven conductance fluctuations mentioned above.

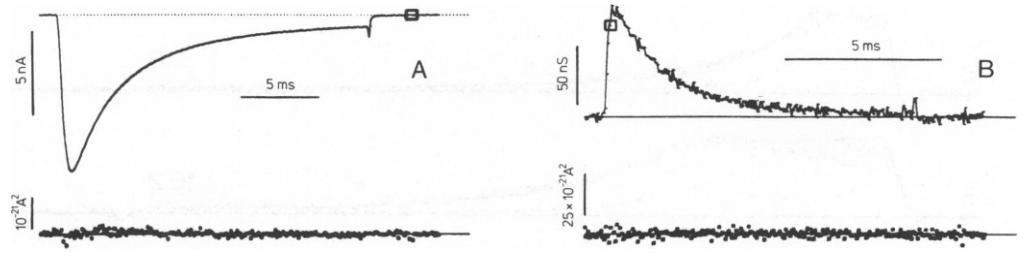

FIGURE 4 Tests for extraneous sources of current fluctuations. (*A*) Mean current time-course (upper) and one projection of the covariance $C(t_1,t_2)$ plotted as a function of t_2. The covariance was evaluated at a reference time t_1, indicated by the box on the mean trace, chosen to be after the end of the depolarization. Node 30; 65 groups of six depolarizations to -5 mV preceded by -105-mV prepulses. The covariance was averaged with $w = 8$. Note the single point from the background fluctuations and the absence of features at the time of peak current. (*B*) Fluctuations at the reversal potential. Upper trace is the approximate time-course of g_{Na}, evaluated by subtracting records obtained with depolarizations to +48 and +68 mV after prepulses to -105 mV. Lower trace is the covariance at 48 mV evaluated near the time of the peak conductance. Node 28; 64 groups of four records. 5-kHz filter bandwidth and 100-μs sample intervals were used in both cases.

The fluctuations therefore appear to arise from the sodium current, and are apparently not due to coherent perturbations in the whole population of channels. In the analysis that follows it is assumed that the fluctuations arise only from the background noise and fluctuations in the number of open channels. Shot noise and other fluctations in the current through open channels have been assumed to be either negligible or contained in the spike at $t_2 = t_1$, which is ignored.

Experimental p_{11} Functions

Fig. 5 shows the mean current record and p_{11} evaluated at four different values of the reference time t_1 from a set of tail currents. While the decay of p_{11} for $t_2 > t_1$ resembles the time-course of the mean current for t_1 chosen early in the test pulse (t_1 = 0.4 and 1.4 ms), the decay is clearly slower for t_1 chosen later in the pulse. A similar change in the decay is seen in

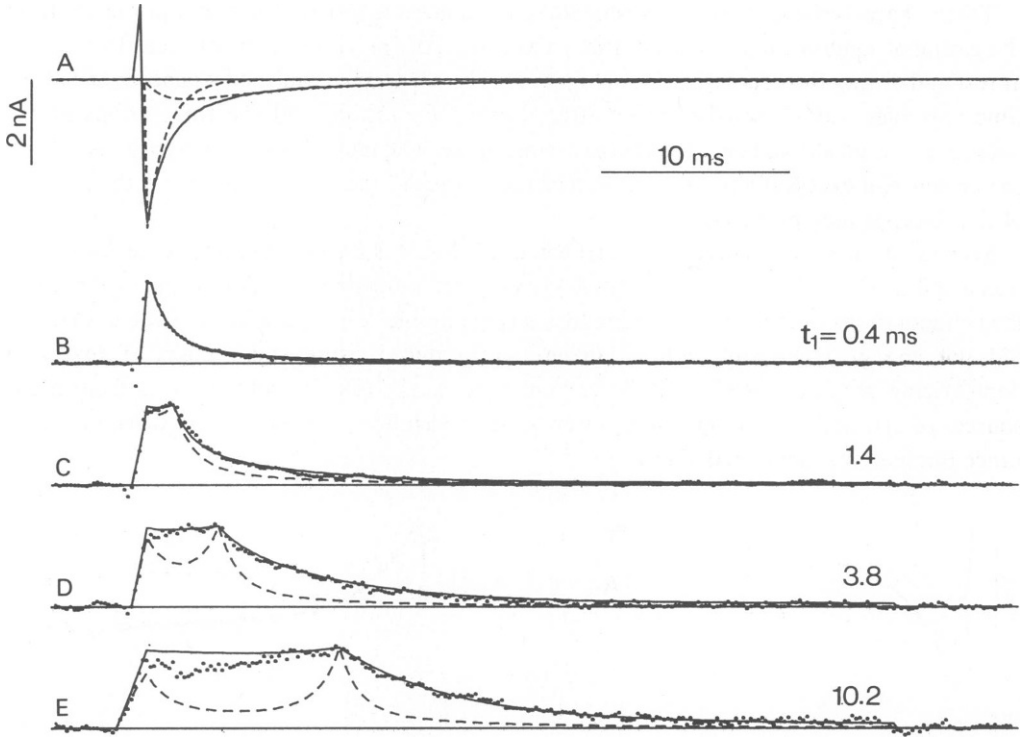

FIGURE 5 Conditional probability in a tail-current experiment. (*A*) Mean current; (*B–E*) four projections of the conditional probability p_{11} $(t_2|t_1)$ evaluated at the t_1 values shown to the right and plotted as a function of t_2. The pulse pattern was a 50-ms prepulse to -105 mV, a 0.4-ms activating pulse to +125 mV, and a 39.6-ms test pulse at +5 mV. Fiber 56. Fluctuations were analyzed in 100 groups of four records. p_{11} values were calculated from covariance projections (Eq. 13) with i = -0.35 pA and N = 20,000. The dashed curves in *A* are the predictions of scheme C for the current carried by channels in the two different open states. Superimposed on the data in *B–E* are predictions of scheme A (dashed curve) and B. The slow initial rising phases arise from the averaging widths, which were 0.4, 0.8, 0.8, and 1.6 ms, respectively, in *B*, *C*, *D*, and *E*. The kinetic parameters for both schemes were λ_1^{-1} = 0.5 ms, λ_2^{-1} = 1.1 ms, λ_3^{-1} = 6.1 ms, b_2/b_3 = 3.6, b_0 = 0.012. The rate constants (ms^{-1}) for scheme A were α_m = 1.9, β_m = 0.04, α_1 = 0.15, β_1 = 0.71, α_2 = 0.015, β_2 = 0.19; for scheme B, α_m = 1.9, β_m = 0.06, β_o = 0.80, β_1 = 0.17, α_2 = 0.010, β_2 = 0.155.

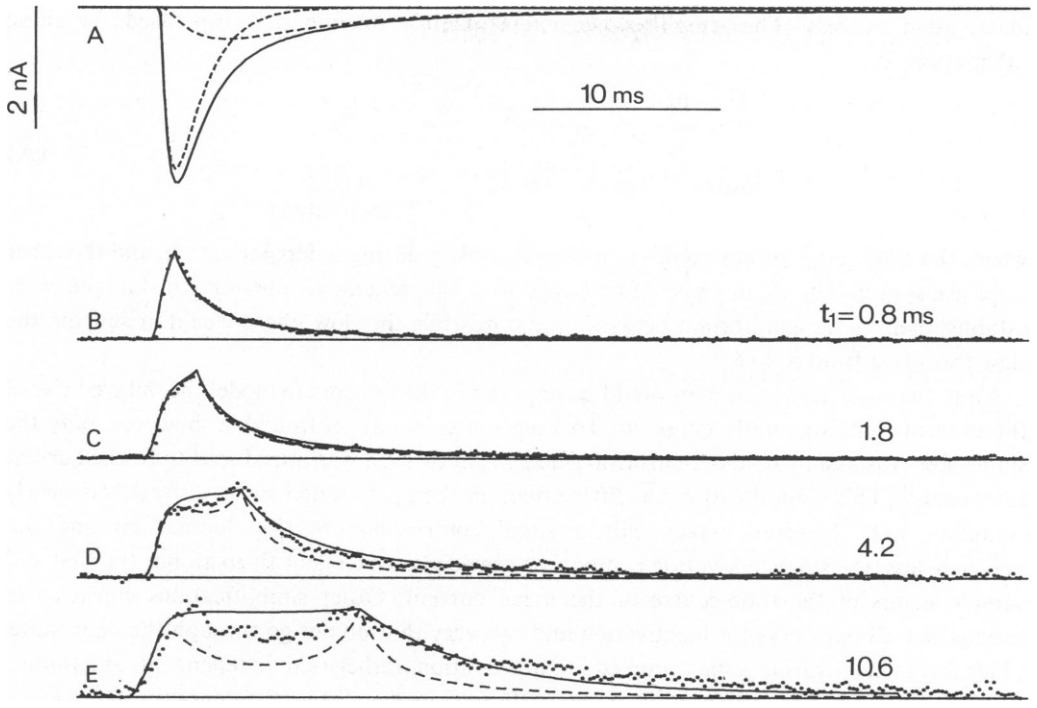

FIGURE 6 Conditional probability during step depolarizations. (*A*) Mean current; (*B–E*) conditional probability $p_{11}(t_2|t_1)$ evaluated at the t_1 values shown with i = -0.52 pA, N = 10,000. Same fiber as in Fig. 5, but currents were recorded after application and partial washout of 200 nM TTX. 50-ms prepulses to -105 mV were followed by 40-ms depolarizations; 45 groups of four records were analyzed. Predictions of scheme A and C are shown as in Fig. 5. The kinetic parameters were λ^{-1}_1 = 0.46 ms, λ^{-1}_2 = 1.6 ms, λ^{-1}_3 = 6.1 ms, b'_1/b'_3 = 4.0, b'_0 = 0.01. Rate constants (ms^{-1}) for scheme A were α_m = 2.0, β_m = 0.04, α_1 = 0.083, β_1 = 0.52, α_2 = 0.013, β_2 = 0.19; for scheme B, α_m = 2.0, β_m = 0.06, β_0 = 0.59, β_1 = 0.12, α_2 = 0.008, β_2 = 0.16.

p_{11} from step depolarizations to the same potential in the same fiber (Fig. 6). Between the runs of Figs. 5 and 6, 200 nM TTX was applied to the fiber and then washed off. Because of incomplete washout, the currents in Fig. 6 were smaller and the value of N decreased, but the value of i increased. A comparison with a set of identical step depolarizations taken before the TTX treatment, however, showed no change in kinetics or in the form of p_{11}.

Superimposed for comparison with the data in Figs. 5 and 6 are the predictions of two simplified kinetic schemes for Na channel gating. These schemes are intended only as examples to provide some insight into the meaning of the observed p_{11} functions; more data and more complex schemes would be required to describe p_{11} in a well-constrained theory. The two schemes were chosen to predict the same mean-current time-course, and to have as many parameters as possible determined by that time-course, while having different kinds of inactivation processes.

A One-Open-State Theory

The first scheme is based on the theory of Chiu (1977), which accounts for a two-component inactivation time-course by assuming two distinct closed states but only one open state in the

inactivation process. The simplified version of Chiu's scheme that was used for these calculations is

$$\underset{\text{closed}}{m} \underset{\alpha_m}{\overset{\beta_m}{\rightleftharpoons}} \underset{\text{open}}{x} \underset{\beta_1}{\overset{\alpha_1}{\rightleftharpoons}} \underset{\text{closed}}{h_1} \underset{\beta_2}{\overset{\alpha_2}{\rightleftharpoons}} \underset{\text{closed (inactivated)}}{h_2} \qquad \text{(A)}$$

where the single activation step $m \rightarrow x$ proceeds rapidly during a depolarization, and the other steps are slower. The rapid phase of inactivation in this scheme can be imagined as the early establishment of an equilibrium between x and h_1 while the slow phase would arise from the slow transition from h_1 to h_2.

More than one activation step would be required in this scheme to model the delayed rise of the current that is actually observed. To keep the calculations tractable, however, only the single step was assumed, and an arbitrary delay t_d in turn-on was introduced to fit the current time-course. This simplification has little effect on the p_{11} function since activation is nearly complete, and therefore makes only a small contribution to the fluctuations and p_{11}. Nevertheless, the single activation component provided an excellent fit to all but the first 1–2 sample points of the time-course of the mean current. Other simplifications consisted of leaving out all pathways for inactivation and recovery that do not go through the open state. (This forces inactivation to be "coupled" to inactivation, rather than independent, as assumed by Chiu, 1977.) The absence of these pathways makes little difference in the kinetic predictions for currents and p_{11} during depolarizations, but reduces the number of parameters to be determined in the theory.

In this scheme the probability of channels being open during a tail current or a step depolarization are of the form

$$p_{(\text{tail})}(t) = b_0 + \sum_{i=1}^{3} b_i \exp(-\lambda_i t) \qquad (16)$$

$$p_{(\text{step})}(t) = b_0' + \sum_{i=1}^{3} b_i' \exp(-\lambda_i t), \qquad (17)$$

where the three relaxation rates are the activation rate $\lambda_1 = 1/\tau_m$ and the two inactivation rates λ_2 and λ_3. $p_{(\text{tail})}$ and $p_{(\text{step})}$ are calculated as the probabilities $p_x(t)$ of being in the open state x given the respective initial conditions $p_x(0) = 1$ or $p_m(0) = 1$.

The first step in computing p_{11} for this scheme was to fit the mean-current time-course $I(t)$ to Eq. 16 or 17 using the relation $p(t) = I(t)/(Nip_0)$ to obtain suitably normalized values for $p(t)$. The normalization factor p_0 was left as a free parameter (it had values between 0.5 and 0.8). This was necessary because, in the experiments, smaller fractions of channels were opened than predicted from scheme A and the chosen initial conditions. In the case of tail currents this was partly due to inactivation during the short activating pulse. In both pulse patterns inactivation pathways that do not pass through the open state would also reduce the fraction of channels that open; since these pathways are ignored in this scheme their effect is included in p_0.

Because of the normalization and initial conditions, fits to Eqs. 16 and 17 have five or six independent kinetic parameters. In the case of tails, all of the rate constants can in principle be determined by a fit to Eq. 16. In practice, however, the activation rate λ_1, because its

component was very small, was "borrowed" from the fit to $p_{(step)}$, and the amplitude b_1 was assumed to be 0.1. The rate constants were calculated from the λ_i and b_i or b_i' using an approximate solution of the equations describing scheme A. Substitution of the rate constants into the equations then allowed solutions to be calculated for different initial conditions.

The initial condition $p_{(tail)}(0) = 1$ is the condition for computing p_{11}; therefore the decay of p_{11} is the same as the tail-current time-course,

$$p_{11}(t_2 | t_1) = p_{(tail)}(t_2 - t_1), \qquad t_2 \geq t_1. \tag{18}$$

Given this decay function, the rest of p_{11} was then calculated according to Eq. 7. This prediction for p_{11} is shown as the dashed lines in Figs. 5 and 6. In the case of the tail currents (Fig. 5), there was actually no need for fitting at all, since p_{11} could have been computed directly from the normalized current time-course and Eq. 18. The only contributions from the theory were, first the assumption of one open state, and second, the assumed initial condition of all channels being in the open state at $t = 0$. The computations for Fig. 6 were more crucially dependent on the form of the reaction scheme, because it was the scheme that allowed the conversion of the measured amplitudes b_i' into the amplitudes b_i corresponding to the different initial conditions. Once the b_i were known, p_{11} was then computed according to Eqs. 18 and 7, as before.

Two Open States

The predictions of scheme A for P_{11} agree well with the experimental data for early reference times t_1, but at later times ($t_1 \geq 1.4$ ms in Fig. 5 and $t_1 \geq 4.2$ ms in Fig. 6) the experimental decay is slower. The two-component fits to the inactivation time-course suggest a way that the decay of p_{11} could be changing: the amplitude of the fast component in p_{11} (which has time constants $\lambda_2^{-1} = 1.1$ and 1.6 ms in Figs. 5 and 6) could be decaying quickly in t_1, perhaps with the same time constant, leaving only the slower inactivation component ($\lambda_3^{-1} = 6.1$ ms) at later times. One scheme that would show this behavior is

$$\begin{array}{ccccc} m_1 & \rightleftarrows & x_1 & \rightarrow & h_1 \\ \downarrow\uparrow & & & & \\ m_2 & \rightleftarrows & x_2 & \rightleftarrows & h_2 \\ \text{resting} & & \text{open} & & \text{inactivated} \end{array} \tag{B}$$

where a slow equilibrium step $m_1 \rightleftarrows m_2$ chooses between two pathways for activation and inactivation. The rapid and irreversible step $x_1 \rightarrow h_1$ gives rise to the fast inactivation component. It also causes the rapid component to disappear rapidly from p_{11}, since in this case p_{11} is the weighted average of the conditional probabilities for each open state (Eq. 9) with the weights being the probabilities p_{x_1} and p_{x_2} of being in the states x_1 and x_2.

Some other two-open-state schemes show the same kind of behavior. The one used for calculations in this work was

$$\begin{array}{ccccccc} & & & h_1 & & h_2 & \text{inactivated} \\ & & & \beta_o \nearrow\!\!\!\!\!\!\searrow \alpha_o & & \beta_2 \nearrow\!\!\!\!\!\!\searrow \alpha_2 & \\ & & \beta_m & & \alpha_1 & & \\ m & \rightleftarrows & & x_1 & \rightleftarrows & x_2 & \\ & & \alpha_m & & \beta_1 & & \\ \text{closed} & & & \text{open} & & \text{open} & \end{array} \tag{C}$$

which was chosen because of its similarity to part of the scheme of Armstrong and Bezanilla (1977), and because it can duplicate the mean-current time-course of scheme A while having a minimum number of nonzero rate constants. Making the transitions $x_1 \rightarrow h_1$ and $x_1 \rightarrow x_2$ irreversible ($\alpha_0 = 0$ and $\alpha_1 = 0$) during a depolarization allows all six of the remaining rate constants to be determined uniquely from fits to Eq. 16, as was the case for scheme A. The irreversible transitions away from x_1 gives p_{11} the property that the fast component vanishes at large t_1 values, as in scheme B. Like scheme A, the pathways that allow unopened channels to inactivate and allow recovery from inactivation are missing; their presence would introduce unconstrained parameters but would probably have only small effects on the predicted kinetics.

The computation of p_{11} for scheme C is detailed in the Appendix. Briefly, the procedure started with the same fit to the mean current time-course that was used for scheme A, which gave three amplitudes and three rates. From these the six rate constants were calculated, whose numerical values are given in the legends of Figs. 5 and 6. From the rate constants five functions were calculated: the open-state probabilities $p_{x_1}(t)$ and $p_{x_2}(t)$, and three conditional probabilities $p_{x_1x_1}(\tau \mid 0)$, $p_{x_2x_1}(\tau \mid 0)$, and $p_{x_2x_2}(\tau \mid 0)$. (The fourth function, $p_{x_1x_2}$, is zero because α_1 is zero.) In the case of tail currents, because of the choice of the initial condition $p_{x_1}(0) = 1$, only three functions needed to be calculated, since $p_{x_1}(t) = p_{x_1x_1}(t \mid 0)$ and $p_{x_2}(t) = p_{x_2x_1}(t \mid 0)$. Finally, p_{11} was computed according to Eq. 9, specifically

$$p_{11}(t_1 + \tau \mid t_1) = \frac{p_{x_1}(t_1)[p_{x_1x_1}(\tau \mid 0) + p_{x_2x_1}(\tau \mid 0)] + p_{x_2}(t_1)p_{x_2x_2}(\tau \mid 0)}{p_{x_1}(t_1) + p_{x_2}(t_1)}, \quad \tau \geq 0 \qquad (19)$$

and completed for $\tau < 0$ using Bayes' rule (Eq. 7). The current components that would be carried by each state, $I_{x_1}(t) = Nip_0p_{x_1}(t)$ and $I_{x_2}(t) = Nip_0p_{x_2}(t)$, are plotted as dashed lines in Figs. 5 *A* and 6 *A*.

The resulting p_{11} functions, plotted as solid curves in Figs. 5 and 6, are very similar to those from scheme A at the early times $t_1 = 0.4$ and 0.8 ms. For tail currents the agreement is in fact exact as $t_1 \rightarrow 0$ because the initial conditions are equivalent. At larger values of t_1, the slow component of the decay predominates, matching the experimental p_{11} very well for tail currents (Fig. 5), and not very well, but somewhat better than scheme A for step depolarizations (Fig. 6).

The behavior of the "rising phase" of p_{11}, with $t_2 < t_1$, is poorly described by either theory in Fig. 6. This rising phase actually contains no new information, since for the theories it is derived from the decay phase, and for the experimental p_{11} the content is essentially the same, because the covariance is symmetrical under interchange of the time variables. The experimental rising phase is, however, more affected by errors in the value of N in the computation of p_{11} (Eq. 13) and so may be less reliable than the decay time-course.

Scheme A predicts a large dip in p_{11} $(t_2 \mid t_1)$ under certain conditions with $t_2 < t_1$ (for example, at $t_1 = 10.6$ ms in Fig. 6). This dip can arise in schemes where there is "flickering" between an open and closed state. It can be understood intuitively as follows. At the beginning of the depolarization in this scheme the channels are predominantly in state x; then, after a few milliseconds, they are distributed between x and h_1. The conditional probability, evaluated at a still later time t_1, is concerned only with those channels that happen to be open at t_1. Those channels have a high probability of being open early in the depolarization, but at

intermediate times are flickering between x and h_1; hence the dip. A much smaller dip can also be seen in the predictions of scheme C. This arises because of the nonzero reverse rate constant α_2, which was chosen to describe the small noninactivating component of the current.

Decay of the Joint Probability

The slower decay in p_{11} at later times was consistently observed in other fibers from *R. pipiens*, as well as at the other potentials that were used. Fig. 7 shows data from the experiment of Fig. 5 and from two other fibers. These plots show the coefficients $a_j(t_1)$ of exponentials used to fit the joint probability function

$$p(t_1)p_{11}(t_1+\tau \mid t_1) = a_0(t_1) + \sum_j a_j(t_1)\exp(-\lambda_j\tau),\ \tau \geq 0. \tag{20}$$

The smallest rate λ_3 was chosen for a single-exponential fit to the decay at late times t_1, and it and one other decay rate were used to provide a best-fit to the tail-current time-course, as in Eq. 11. A third, rapidly-decaying component was needed at -5 mV (Fig. 7 *B*). This component

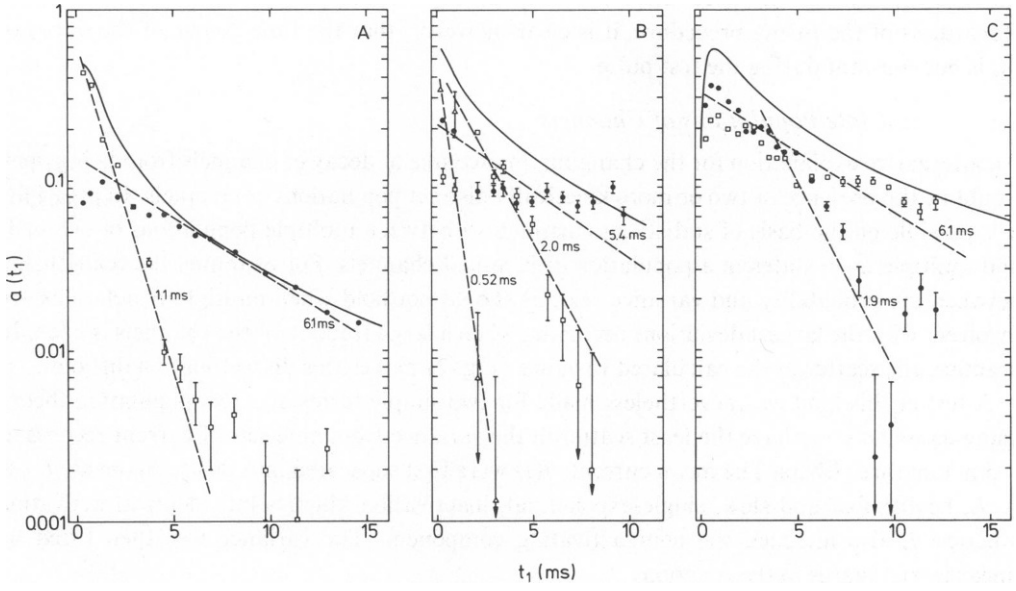

FIGURE 7 Comparison of the probability of channel being open $p(t_1)$ with the coefficients $a_j(t_1)$ of the fitted joint probability functions (Eq. 18), plotted as function of t_1. (*A*) From tail currents at +5 mV; same data set as in Fig 5. Time constants corresponding to the plotted amplitudes were 6.1 ms (●) and 1.1 ms (□). (*B*) Tail currents in fiber 58 at -5 mV, after a prepulse to -105 mV and a 0.2-ms activating pulse to +125 mV. Three components were necessary to fit the decay of the joint probability and the mean current: 5.45 ms (●), 2.0 ms (□), and 0.52 ms (△). (*C*) Currents from depolarizations to -5 mV in a *R. pipiens* fiber. Same data set as in Fig. 3. Time constants were 6.1 ms (□) and 1.9 ms (●). Error bars are ± standard error estimated from equally weighted least-squares fits of these components and a constant term. The constant terms a_0 showed little time dependence, and averaged 0.002 in *A*, 0.008 in *B*, and 0.006 in *C*. The dashed lines show the decay rate of each component; in scheme C the corresponding amplitudes should decay at these rates.

was, surprisingly, slower than τ_m. A fast decay component with a time constant near τ_m was not apparent at +5 mV, so only the two inactivation components were fitted.

For tail currents the form of the joint probability function (Eq. 20) is simply described by schemes A and C. In scheme A the coefficients a_j are each proportional to $p(t_1)$, which is shown as a smooth curve in each part of the figure. The coefficients that correspond to the two inactivation components in scheme C are given in the Appendix. They have the approximate forms

$$a_2(t_1) \simeq c_2 \exp(-\lambda_2 t_1)$$
$$a_3(t_1) \simeq c_0 + c_3 \exp(-\lambda_3 t_1), \tag{21}$$

so that the coefficient a_1 of the faster component decays with the same time constant in t_1 as the component itself decays in τ. Decays in t_1 with the corresponding time constants are shown as dashed lines in the figure. The faster components are seen to decay more quickly than the slow ones, but the agreement with this prediction of scheme C is not complete.

The choice of the time constants in these fits was somewhat arbitrary, especially in the case of Fig. 7 *B*, where three exponentials were used. Also, different time constants were necessary to fit the kinetics of $p_{(\text{depol})}$ and $p_{(\text{tail})}$ in Figs. 5 and 6 from the same fiber, which suggests that the two-exponential fits used there are only a rough approximation to the true kinetics. Regardless of the fitting procedure, it is clear, however, that the time-course of the decay of p_{11} is not constant during the test pulse.

Multiple Populations of Channels

An alternative explanation for the changing time-course of decay of channels from being open would be the presence of two or more kinetically distinct populations of channels. In principle, it is possible on the basis of statistics to distinguish between multiple populations of channels and multiple open states in a population of identical channels. For example, the relationship between the probability and variance (Eq. 5) should not hold when multiple populations are involved, with the largest deviations occurring when a large fraction of the channels is open. In practice, the scatter in the calculated variance (Fig. 2) makes this discrimination difficult.

A test of this kind was nevertheless made for two simple forms of a two-population theory using data chosen to have the least scatter in the variance from nine sets of current records at −5 mV in three fibers. The mean currents $I(t)$ were first separated into two components $I = I_f + I_s$, having fast and slow, single-exponential, inactivation kinetics but identical activation kinetics. I_s also included the noninactivating component. The variance was then fitted by linear least-squares to the functions

$$\sigma^2 \simeq iI + bI^2 + c \qquad N = -1/b \tag{22}$$

$$\left.\begin{aligned}\sigma^2 &\simeq i(I_f + I_s) + b_f I_f^2 + b_s I_s^2 + c \\ \sigma^2 &\simeq i_f I_f + i_s I_s + b_f I_f^2 + b_s I_s^2 + c\end{aligned}\right\} \quad N = -1/b_f;\ N_s = -1/b_s \tag{23, 24}$$

which correspond to one population, two populations N_f and N_s with identical values for the single-channel currents i, and two populations with different values for i.

In four of the nine sets of data the fit to Eq. 23 gave higher total χ^2 values than the fit to Eq. 22. In the remaining five sets the fit to Eq. 23 required nonphysical (positive or near zero) values for b_f, including its error band. In one of the fits to the less constrained Eq. 24 the total

χ^2 was larger than the fit to Eq. 20. In all but one of the others, nonphysical values for one or more of the parameters (usually b_f) were required. Although this analysis would have been better performed with fits constrained to physical values, it can be concluded that these two-population models do not provide a better description of the variance-mean relationship than the one-population theory.

Two of the limitations of this kind of analysis should be kept in mind. First, only one of the many possible ways of "dividing up" the current among populations was tried. Second, the change with time of the spectral characteristics of the noise might lead to a distortion of the time-course of the variance because of the limited filter bandwidth. For these reasons the question of multiple populations of channels might not be answerable except by the observation of currents in single channels.

DISCUSSION

The main result of this work can be expressed as follows. Sodium channels that are open late in a depolarization tend to stay open longer than channels that are open earlier. This effect was seen in both species of frogs used. One explanation for this behavior would be that each channel has several kinetically distinct open states. Two simplified theories for channel gating that predict the same mean-current time-course were presented, one having one open state and the other, two. The failure of the one-open-state theory is representative of the failure of that whole class of theories. This is because, given the assumption that gating is a time-homogeneous Markov process, these theories all predict a constant time-course of decay of p_{11}. The relative success of the two-open-state theory does not, however, rule out the the possibility of more open states, or of an entirely different kinetic scheme. The presence of three or more relaxations in the decay under some conditions, as well as the discrepancies in the predictions of the two-open-state theory, suggest that the kinetics are in fact more complicated.

Another explanation for the change in the time-course of the decay would be the presence of multiple populations of channels having different kinetics. One specific theory has been considered in which two populations having identical activation kinetics each show a single inactivation time constant. Although this theory was relatively unsuccessful, other possibilities can be imagined that would describe both the observed p_{11} functions and the variance-mean relationship. An example would be a two-population theory in which the smaller population shows both slower inactivation and slower activation processes; the slow activation would make the presence of the second population difficult to detect in the variance-mean relationship. If there were multiple populations of channels they would need to have similar single-channel conductances, reversal potentials, and TTX affinities to be consistent with other data, including the variance-mean relationship and the existence of a reversal potential. Note that, while Goldman and Hahin (1978) report a change in kinetics with TTX in *Myxicola* axons, such a change is not apparent in frog node (see, for example, Sigworth, 1980*b*). Finally the observed changes with potential of the relative amplitudes of the fast and slow inactivation components may be difficult to explain in a two-population theory.

Short-term Drift in the Clamped Potential

The change in gating kinetics with time could conceivably arise from a consistent drift in the clamped membrane potential. An effect of this kind may occur in the node of Ranvier voltage

clamp, as evidenced by unusual current kinetics sometimes seen near the reversal potential, especially under conditions that slow inactivation. This effect is probably due to a time-dependence in the attenuation artifact (C. F. Stevens and F. Sigworth, unpublished observations; Dodge and Frankenhaeuser, 1958) which causes the change in clamped membrane potential to increase slowly ($\tau \sim 10$ ms) after a potential jump. This effect was relatively small in the *R. catesbiana* fibers, as evidenced by a smooth reversal of the currents; these fibers also had smaller slow components (Dodge and Frankenhaeuser, 1959) in the capacitance transient. It also operates in the wrong direction, causing an increased depolarization during a step depolarization, which would tend to cause an acceleration rather than a slowing of inactivation kinetics. It was roughly 2% in magnitude in fiber 56, judging from the reversal potential trace in Fig. 1, which would result in only a 3-mV drift during the pulse.

Previous Evidence for Multiple Open States of the Sodium Channel

Frankenhaeuser and Hodgkin (1957) presented data which suggest the presence of multiple open states. They recorded tail currents in a squid axon in a low Mg^{++}, high Ca^{++} solution and found an increase followed by a decrease in the apparent time constant of the tails as the duration of the activating pulse was increased. Goldman and Hahin (1978) have made a careful study of such initial-condition effects on tail currents in *Myxicola* at normal Ca^{++} levels. They find a change with prepulse duration in the relative magnitude, but not time constants, of the several relaxation components in the tail time-course. A similar effect can be seen in the node of Ranvier (Fig. 8); with longer activating pulses a larger slow component of the tail time-course is visible. A simple explanation for this behavior would be the existence of multiple open states of the channel, which show different decay times at the repolarizing potential.

This interpretation is, however, complicated by the (unknown) degree of loading of closed states at the end of the activating pulse. Varying populations of closed states could influence the time-course of tail currents if channels that are closed at the beginning of the

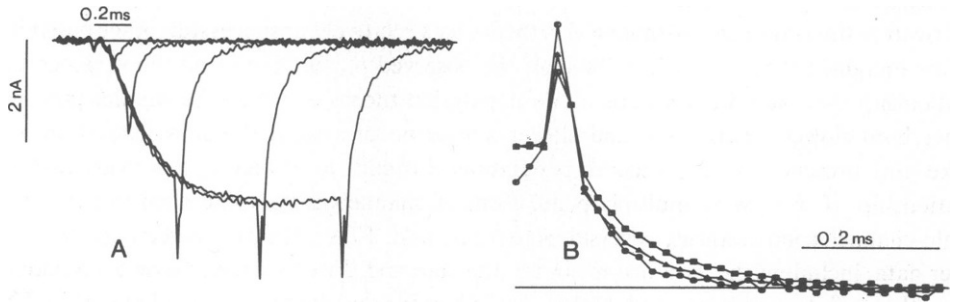

FIGURE 8 Change in the time-course of tails with activating-pulse duration. (*A*) Superimposed current records from activating pulses to -5 mV returning to -65 mV after 0.1, 0.2, 0.5, 1.0, and 1.5 ms. Depolarizing prepulses (10-ms to -65 mV) reduced the current amplitude to minimize series-resistance effects; series resistance compensation (260 kΩ) was also used. Fiber 29. Current-monitor signal was filtered at 20 kHz, Bessel response. (*B*) Normalized time-courses of the tail currents in *A* after 0.2-ms (○), 0.5-ms (▲), and 1.5-ms (□) activating pulses. The tail currents were normalized according to the value 20 μs after repolarizing. Node 29.

repolarization can open during the course of the tail current. Thus, it is also possible to explain changes in the tail time-course by a complex gating scheme with only one open state; this is the approach taken by Goldman and Hahin. This ambiguity does not occur with the conditional probability functions presented in this paper because p_{11} is, by definition, concerned only with channels that are open at a reference time, and channels that open subsequently are ignored.

Chandler and Meves (1970 *a,b*) concluded that a second open state in the inactivation process was responsible for the large substained currents observed at large depolarizations in squid axons perfused with fluoride solutions. If a state with the same kinetics existed in node of Ranvier channels it would not be highly populated, since at +125 mV the noninactivating component was only 6 % of the peak current, and in the range of the test potentials used here, -15 to +5 mV, it was smaller than 4%. It would contribute only a small component to the joint probability function, and the amplitude of this component would be constant, rather than decaying with time.

Armstrong and Benzanilla (1977; see also Armstrong and Gilly, 1979) introduced a scheme with two adjacent open states to explain gating current phenomena. Because they saw a gating current component that was slower than the initial activation process, they postulated a transition involving the movement of gating charge that occurs while the channel is open. The data presented in this paper are consistent with this kind of theory, but do not rule out other configurations of open states. An example of an extreme alternative is the electrodiffusion model of gating proposed by Neumcke et al. (1978), also based on gating current observations. In this model there is an infinite number of open "states", defined by a region in diffusion space.

Comparison with Stationary Noise Analysis Results

The nonstationary fluctuation analysis technique has been exploited in this work to look for changes, with time, of the spectral characteristics of Na current fluctuations.The stationary covariance and power spectrum, because they are calculated as time averages, do not allow such changes on short time scales to be seen. Note, however, that for stationary fluctuations the covariance evaluated in this work and the usual stationary covariance have exactly the some form (Eq. 8).

The change in the decay from the open state during the course of a depolarization suggests that previous determinations of power spectra from sodium current fluctuations (Conti et al., 1980, 1976., 1975; Fishman et al., 1976) may reflect only one of several gating modes for the channels. Since the spectra were obtained very late ($t_1 > 190$ ms) during depolarizations, they might not have a simple relationship to the kinetics of the mean current earlier in the depolarization. For example, the present work shows that a spectrum obtained in this way near 0 mV would lack the fast inactivation component that dominates the time-course of the mean current. A direct comparison between earlier work and the results presented here is unfortunately not possible because the potential ranges studied do not overlap. On the other hand, from the present work there is no reason to expect a change in channel conductance during depolarization. The correspondence in single-channel current estimates obtained by the stationary and nonstationary techniques (Conti et al., 1980; Sigworth, 1980*a*) supports this view.

I wish to thank Professor C. F. Stevens for his support and encouragement of this work, most of which was done in his laboratory and under U.S. Public Health Service grant No. 12962. I also thank Dr. E. Neher, in whose laboratory the analysis was completed, and the Alexander von Humboldt-Stiftung for financial support during this period.

Received for publication 22 April 1980 and in revised form 8 September 1980.

APPENDIX

Calculation of p_{11} for the Two-Open-State Scheme C

The first step is to solve the kinetic equations to give expressions relating the rate constants to the amplitudes b_i and rates λ_i of the various relaxations of the mean current. The λ_i and b_i are obtained by fitting the mean-current time-course to Eqs. 16 or 17. The kinetic equations are

$$\frac{\mathrm{d}}{\mathrm{d}t}\begin{bmatrix} p_m \\ p_{x_1} \\ p_{h_1} \\ p_{x_2} \\ p_{h_2} \end{bmatrix} = \begin{bmatrix} -\alpha_m & \beta_m & 0 & 0 & 0 \\ \alpha_m & -\beta & \alpha_0 & \alpha_1 & 0 \\ 0 & \beta_0 & -\alpha_0 & 0 & 0 \\ 0 & \beta_1 & 0 & -\alpha_1-\beta_2 & \alpha_2 \\ 0 & 0 & 0 & \beta_2 & -\alpha_2 \end{bmatrix} \begin{bmatrix} p_m \\ p_{x_1} \\ p_{h_1} \\ p_{x_2} \\ p_{h_2} \end{bmatrix} \tag{1}$$

where $\beta = \beta_m + \beta_0 + \beta_1$. The probabilities p_m, p_{x_1}, etc., of being in each state are nonnegative and sum to 1.

The assumption that $\alpha_0 = 0$ and $\alpha_1 = 0$ allows Eq. 1 to be solved analytically by uncoupling the equations into three systems,

$$\frac{\mathrm{d}}{\mathrm{d}t}\begin{bmatrix} p_m \\ p_{x_1} \end{bmatrix} = \begin{bmatrix} -\alpha_m & \beta_m \\ \alpha_m & -\beta \end{bmatrix} \begin{bmatrix} p_m \\ p_{x_1} \end{bmatrix} \tag{2a}$$

$$\frac{\mathrm{d}}{\mathrm{d}t} p_{h_1} = \beta_0 p_{x_1} \tag{2b}$$

$$\frac{\mathrm{d}}{\mathrm{d}t}\begin{bmatrix} p_{x_2} \\ p_{h_2} \end{bmatrix} = \begin{bmatrix} \beta_1 p_{x_1} \\ 0 \end{bmatrix} + \begin{bmatrix} -\beta_2 & \alpha_2 \\ \beta_2 & -\alpha_2 \end{bmatrix} \begin{bmatrix} p_{x_2} \\ p_{h_2} \end{bmatrix} \tag{2c}$$

Eq. 2a has two eigenvalues, $-\lambda_1$ and $-\lambda_2$, such that

$$\begin{aligned} \lambda_1 + \lambda_2 &= \alpha_m + \beta_m + \beta_0 + \beta_1 \\ \lambda_1\lambda_2 &= \alpha_m(\beta_0 + \beta_1). \end{aligned} \tag{3a}$$

Since α_m is relatively large, $\lambda_1 \simeq \alpha_m + \beta_m$ and corresponds to the activation rate. λ_2 is the faster inactivation rate. The slower inactivation rate is the nonzero eigenvalue from Eq. 2c,

$$\lambda_3 = \alpha_2 + \beta_2 . \tag{3b}$$

The time-course of the probability $p_{jk}(t\,|\,0)$ for any state j, given the initial condition of state k at time zero, is of the form

$$p_{jk}(t\,|\,0) = a_0 + \sum_i a_i \, \mathrm{e}^{-\lambda_i t}, \tag{4}$$

and the remainder of the solution procedure is to find the coefficients a_i. Expressions for all of the coefficients relevant to computing p_{11} are given in Table I. Since the mean-current time-course is

TABLE I

COEFFICIENTS (EQ. 4) FOR $p_{jk}(t|0)$

Function	Initial condition	Coefficients			
		a_0	a_1	a_2	a_3
$p_{x_1m} = p_{x_1(\text{step})}$	$p_m(0) = 1$	0	$\dfrac{-\alpha_m}{\Delta_{12}}$ -1.723	$\dfrac{\alpha}{\Delta_{12}}$ 1.723	0
$p_{x_2m} = p_{x_2(\text{step})}$	$p_m(0) = 1$	$\dfrac{\alpha_m\alpha_2\beta_1}{\lambda_1\lambda_2\lambda_3}$ 0.012	$\dfrac{\alpha_m\beta_1(\lambda_1 - \alpha_2)}{\lambda_1\Delta_{12}\Delta_{13}}$ 0.154	$\dfrac{-\alpha_m\beta_1(\lambda_2 - \alpha_2)}{\lambda_2\Delta_{12}\Delta_{23}}$ -0.378	$\dfrac{\alpha_m\beta_1\beta_2}{\Delta_{13}\Delta_{23}\lambda_3}$ 0.212
$p_{x_1x_1} = p_{x_1(\text{tail})}$	$p_{x_1}(0) = 1$	0	$\dfrac{\lambda_1 - \alpha_m}{\Delta_{12}}$ 0.110	$\dfrac{\alpha_m - \lambda_2}{\Delta_{12}}$ 0.890	0
$p_{x_2x_1} = p_{x_2(\text{tail})}$	$p_{x_1}(0) = 1$	$\dfrac{\alpha_m\alpha_2\beta_1}{\lambda_1\lambda_2\lambda_3}$ 0.012	$\dfrac{-\beta_1(\lambda_1 - \alpha_2)(\lambda_1 - \alpha_m)}{\lambda_1\Delta_{13}\Delta_{12}}$ -0.010	$\dfrac{-\beta_1(\lambda_2 - \alpha_2)(\alpha_m - \lambda_2)}{\lambda_2\Delta_{12}\Delta_{23}}$ -0.195	$\dfrac{\beta_1\beta_2(\alpha_m - \lambda_3)}{\lambda_3\Delta_{13}\Delta_{23}}$ 0.193
$p_{x_2x_2}$	$p_{x_2}(0) = 1$	$\dfrac{\alpha_2}{\lambda_3}$ 0.070	0	0	$\dfrac{\beta_2}{\lambda_3}$ 0.930

General expressions are given as well as numerical values based on the fit to the mean current in Fig. 5, where the relaxation rates were $\lambda_1 = 2.0$, $\lambda_2 = 0.91$, and $\lambda_3 = 0.16$ ms^{-1}. The parameters Δ are defined as $\Delta_{ij} = \lambda_i - \lambda_j$.

proportional to $p_{x_1} + p_{x_2}$, the three equations (3a) and (3b) plus three of the four equations for the coefficients of $p_{x_1} + p_{x_2}$ allow the six nonzero rate constants to be calculated. From the values of the rate constants all of the remaining coefficients can be calculated. Numerical values for the coefficients are given in the Table, obtained by back-substituting the rate constants from Fig. 5 in this way.

Given the coefficients, the conditional probability p_{11} can then be calculated from the individual functions (Eq. 4) according to Eq. 19 in the text. The numerator in this expression is the joint probability of being in an open state at both t_1 and $t_1 + \tau$. For tail currents it has the form

$$p_{\text{joint}}(t_1, t_1 + \tau) = p_{x_1x_1}(t_1|0)[p_{x_1x_1}(\tau|0) + p_{x_2x_1}(\tau|0)] + p_{x_2x_1}(t_1|0)p_{x_2x_2}(\tau|0). \quad (5)$$

From the numerical values in the Table the expression becomes

$$\begin{aligned} p_{\text{joint}}(t_1, t_1 + \tau) = {} & (0.11\, e^{-\lambda_1 t_1} + 0.89\, e^{-\lambda_2 t_1}) \\ & \times (0.01 + 0.1\, e^{-\lambda_1 \tau} + 0.7\, e^{-\lambda_2 \tau} + 0.19\, e^{-\lambda_3 \tau}) \\ & + (0.01 - 0.01\, e^{-\lambda_1 t_1} - 0.2\, e^{-\lambda_2 t_1} + 0.19\, e^{-\lambda_3 t_1}) \\ & \times (0.07 + 0.93\, e^{-\lambda_3 \tau}), \end{aligned}$$

which, on collecting terms, is seen to be approximately

$$p_{\text{joint}}(t_1, t_1 + \tau) \simeq 0.62\, e^{-\lambda_2 t_1} e^{-\lambda_2 \tau} + (0.01 + 0.18\, e^{-\lambda_3 t_1}) e^{-\lambda_3 \tau},$$

with the other terms either decaying quickly (rate λ_1 in t_1 or having coefficients < 0.01. This

approximation is of the form of Eq. 21 in the text, and becomes exact for tail currents when $\beta_m/\alpha_m \gg 0$ and $\alpha_2/\beta_2 \gg 0$; that is, in the limit of complete activation and complete steady-state inactivation.

REFERENCES

ARMSTRONG, C. M., and F. BENZANILLA. 1977. Inactivation of the sodium channel. II. Gating current experiments. *J. Gen. Physiol.* **70**:567–590.

ARMSTRONG, C. M., and W. F. GILLY. 1979. Fast and slow steps in the activation of sodium channels. *J. Gen. Physiol.* **74**:691–711.

BENDAT, J. S., and A. G. PIERSOL. 1971. Random Data: Analysis and Measurement Procedures. Wiley Interscience, New York.

CHANDLER, W. K., and H. MEVES. 1970*a*. Evidence for two types of sodium conductance in axons perfused with sodium fluoride solution. *J. Physiol. (Lond.)*. **211**:679–678.

CHANDLER, W. K., and H. MEVES. 1970*b*. Rate constants associated with changes in sodium conductance in axons perfused with sodium fluoride. *J. Physiol. (Lond.)*. **211**:679–705.

CHIU, S. Y. 1977. Inactivation of sodium channels: second order kinetics in myelinated nerve. *J. Physiol. (Lond.)*. **273**:573–596.

COLQUHOUN, D., and A. G. HAWKES. 1977. Relaxation and fluctuations of membrane currents that flow through drug-operated channels. *Proc. R. Soc. Lond. B.* **199**:231–262.

CONTI, F., and E. WANKE. 1975. Channel noise in nerve membranes and and lipid bilayers. *Q. Rev. Biophys.*. **8**:451–506.

CONTI, F., L. J. DEFELICE, and E. WANKE. 1975. Potassium and sodium ion current noise in the membrane of the sqiud giant axon. *J. Physiol. (Lond.)*. **248**:45–82.

CONTI, F., B. HILLE, B. NEUMCKE, W. NONNER, and R. STÄMPFLI. 1976*a*. Measurement of the conductance of the sodium channel from current fluctuations at the node of Ranvier. *J. Physiol. (Lond.)*. **262**:699–727.

CONTI, F., B. HILLE, B. NEUMCKE, W. NONNER, and R. STÄMPFLI. 1976*b*. Conductance of the sodium channel in myelinated nerve fibres with modified sodium inactivation. *J. Physiol. (Lond.)*. **262**:728–742.

CONTI, F., B. NEUMCKE, W. NONNER, and R. STÄMPFLI. 1980. Conductance fluctuations from the inactivation process of sodium channels in myelinated nerve fibres. *J. Physiol. (Lond.)*. **308**:217–239.

DEFELICE, L. J. 1977. Fluctuation analysis in neurobiology. *Int. Rev. Neurobiol.* **20**:169–208.

DODGE F., and B. FRANKENHAEUSER. 1958. Membrane currents in isolated frog nerve under voltage clamp conditions. *J. Physiol. (Lond.)*. **143**:76–90.

DODGE, F., and B. FRANKENHAEUSER. 1959. Sodium currents in the myelinated nerve fibre of *Xenopus laevis* investigated with the voltage clamp technique. *J. Physiol. (Lond.)*. **148**:188–200.

EHRENSTEIN, G., H. LECAR, and R. NOSSAL. 1970. The nature of the negative resistance in bimolecular lipid membranes containing excitability-inducing material. *J. Gen. Physiol.* **55**:119–133.

FISHMAN, H. M., L. E. MOORE, and D. POUSSART. 1976. Ion movements and kinetics in squid axon. II. Spontaneous electrical fluctuations. *Ann. N.Y.Acad. Sci.* **303**:399–423.

FRANKENHAEUSER, B., and A. L. HODGKIN 1957. The action of calcium on the electrical properties of squid axons. *J. Physiol. (Lond.)*. **137**:218–244.

GOLDMAN, L., and R. HAHIN. 1978. Initial conditions and the kinetics of the sodium conductance in *Myxicola* giant axons. II. Relaxation experiments. *J. Gen. Physiol.*. **72**:879–898.

HILL, T. L., and Y. CHEN. 1972. On the theory of ion transport across the nerve membrane. IV. Noise from the open-close kinetics of K channels. *Biophys. J.* **12**:948–959.

HILLE, B. 1976. Gating in sodium channels in nerve. *Ann. Rev. Physiol.*. **38**:139–152.

NEHER, E., and C. F. STEVENS. 1977. Conductance fluctuations and ionic pores in membranes. *Ann. Rev. Biophys. Bioeng.* **6**:345–381.

NEUMCKE, B., W. NONNER, and R. STÄMPFLI 1978. Gating currents in excitable membranes. *Int. Rev. Biochem.* **19**:129–155.

NONNER, W. 1980 Relations between the inactivation of sodium channels and the immobilization of gating charge in frog myelinated nerve. *J. Physiol. (Lond.)*. **299**:573–603.

PAPOULIS, A. 1965. Probability, Random Variables and Stochastic Processes. McGraw-Hill Book Co., New York. Chapter 12.

SIGWORTH, F. J. 1977. Sodium channels in nerve apparently have two conductance states. *Nature (Lond.)*. **270**:265–267.

SIGWORTH, F. J. 1979. Analysis of nonstationary sodium current fluctuations in frog myelinated nerve. Thesis, Yale University.

SIGWORTH, F. J. 1980*a*. The variance of sodium current fluctuations at the node of Ranvier. *J. Physiol. (Lond.)*. **307**:97–129.

SIGWORTH, F. J. 1980*b*. The conductance of sodium channels under conditions of reduced current at the node of Ranvier. *J. Physiol. (Lond.)*. **307**:131–142.

STEVENS, C. F. 1972. Inferences about membrane properties from electrical noise measurements. *Biophys. J.* **22**:1028–1047.

STEVENS, C. F. 1978. Interactions between intrinsic membrane protein and electric field. *Biophys. J.* **22**:295–306.

VAN DEN BERG, R. J., E. SIEBENGA, and G. DEBRUIN. 1977. Potassium ion noise currents and inactivation in voltage-clamped node of Ranvier. *Nature (Lond.)*. **265**:177–179.